Macromodel for the Mechanics of Gecko Hair Adhesion

Michael P. Reyes and Ronald S. Fearing

Abstract—**In this work, we explore the mechanical behavior of gecko hairs by means of macromodels. The macromodel has four spatular hairs operating by magnetic forces instead of van der Waals forces. The purpose of the models is to simulate the mechanics of the actual gecko seta. For additional hair compliance, a two degree of freedom double bent spatular hair geometry is chosen. A mathematical model for the displacement and forces (slide, peel, and pull-off) for the macro scale gecko hairs is presented. Experiments showed good agreement with the model and a directional adhesion effect which could be useful for locomotion.**

I. Introduction

GECKOS have the ability to climb and run on almost any surface, whether smooth or rough, wet or dry, with very high maneuverability and efficiency. The foot sticking and release mechanisms are the critical components to understand and replicate the gecko's dry adhesive properties [2]. Because they have compliant micro- and nano-scale high aspect ratio beta-keratin structures at their feet, geckos can adhere to any surface with a shear controlled contact area [3]. This adhesion is due to intermolecular forces such as van der Waals force. Since geckos are the largest animals to adhere to almost any surface, gecko mechanics is useful for developing future wall climbing robots, surgical robots and other general dry adhesion applications.

An important feature of gecko mechanics is the "frictional adhesion" effect. In frictional adhesion, the maximum adhesive force is directly proportional to the applied tangential force and the angle of attachment when pulling along the adhesive direction [7, 8].

Currently synthetic hairs are fabricated to mimic the adhesion of actual gecko setae. Since fabricating synthetic hairs is difficult, constructing macromodels of gecko hairs is a means to guide the design of the final nanoscale adhesive. These models are low cost and easy to build. The gecko apparatus from [5] models the entire gecko foot. This physical model represents a highly compliant five fingered nylon hair pad which comprises eight magnetic spatulae made of rare earth neodymium magnets [6]. Each finger represents a setal stalk and each magnet corresponds to a spatula.

In this paper, we use a macromodel of a single setal stalk with 4 magnetic spatulae. In section II, Force limits for peeling, lifting and sliding are derived and compared with experiments. To increase compliance, we chose a double-bent spatular hair geometry. Displacement limits for sliding and peeling are modeled and measured. We assumed a flexural pivot for the spatular displacement. The experimental results and their comparison to the mathematical model are presented in section III. Section IV concludes with a comparison between the macromodel and a frictional adhesion model.

II. Mathematical Model

A. *Force limit for rigid spatular hair array*

We first develop a simple mechanical model to predict the force limit for a single seta. As shown in Fig. 1a, we model a setal stalk containing hundreds of spatular hairs, where the hairs are assumed rigid. This model assumes that all spatulae are in contact with the surface with a uniform adhesive pressure of P_0 expressed in N/m. We assume a Coulomb friction model where $F_t = \mu F_n$ and μ is the coefficient of friction, F_t is the tangential force and F_n is the normal force. A tension T acts at angle ϕ pulling the spatular hairs from the surface. The three possible conditions are sliding, peeling of the seta and lifting (pull-off). From static equilibrium, we can solve for the forces for sliding to the right:

$$T \cdot \cos\phi > \mu \cdot (P_0 \cdot l - T \cdot \sin\phi), \tag{1}$$

and lifting:

$$T \cdot \sin\phi > P_0 \cdot l\,. \tag{2}$$

For peeling of the seta, the moment is taken with respect to the most distal spatula (see Fig. 1a).

$$T \cdot (s+l) \cdot \sin\phi > T \cdot h \cdot \cos\phi + \int_0^l P_0 \cdot x \cdot dx\,. \tag{3}$$

Solving for T from (3), the equation for peeling of the seta is

$$T > \frac{P_0 \cdot l^2}{2} \frac{1}{[(s+l) \cdot \sin\phi - h \cdot \cos\phi]}. \tag{4}$$

Because constructing a model containing a patch of hundreds of spatulae would be impractical, we model a setal stalk consisting of four evenly spaced rigid spatular hairs. Each magnetic tip is attached to the surface with adhesive force F_0 (see Fig. 1b for setal stalk and Fig. 1d for the spatular close-up). From static equilibrium, we can solve for

Manuscript received February 11, 2008

M. P. Reyes is with the Department of Electrical and Computer Engineering, University of California, Davis, CA 95616 USA (phone: 530-792-1504; e-mail: mpreyes@ucdavis.edu).

R. S. Fearing is with the Electrical Engineering and Computer Science Department, University of California, Berkeley, CA 94720 USA, (e-mail: ronf@eecs.berkeley.edu).

forces for sliding right, sliding left, lifting and peeling of the seta. The equation for sliding to the right (+)/left (-) is

$$\pm T\cdot\cos\phi > \mu\cdot\left(4\cdot\left[F_0+\frac{mg}{4}\right]-T\cdot\sin\phi\right). \quad (5)$$

where F_0 is the adhesive force of each magnet in contact with the surface and $mg/4$ is the weight of a single spatula. For peeling of the seta, the moment is taken with respect to the most distal spatula (see Fig. 1b). The equation for peeling of the seta is

$$T\cdot(s+l)\cdot\sin\phi > T\cdot h_0\cdot\cos\phi+\left(F_0+\frac{mg}{4}\right)\cdot l\cdot\frac{n\cdot(n-1)}{6}. \quad (6)$$

Solving for T from (6), with n = 4, the minimum T for peeling of the seta is

$$T > \frac{2\cdot l\cdot\left(F_0+\frac{mg}{4}\right)}{(s+l)\cdot\sin\phi-h_0\cdot\cos\phi}. \quad (7)$$

To disengage the magnet by lifting normal to the surface:

$$T\cdot\sin\phi > 4\cdot\left(F_0+\frac{mg}{4}\right). \quad (8)$$

B. *Force limit for compliant spatular hair array*

Because the previous model does not take into account the height change of the setal stalk with load, we next develop a simple mechanical model to predict the force limit for a single seta comprised of compliant hairs. We assume that each spatular hair is a linear spring.

Using Hooke's Law, we model a setal stalk consisting of four evenly spaced compliant spatular hairs with their magnetic tips attached to the surface (see Fig. 1c). From static equilibrium, we solve for the forces of the compliant spatulae neglecting the effects of peeling, lifting and sliding. The equation for the force in the x-direction is:

$$F_x = T\cdot\cos\phi = 4\cdot k_x\Delta x \quad (9)$$

where Δx is the displacement and k_x is the stiffness in the x-direction.

The equation for the force in the y-direction is:

$$F_y = T\cdot\sin\phi = \sum_{n=1}^{4} k_y\cdot\left(\Delta y+\left(\frac{n-1}{3}\right)\cdot l\cdot\sin\Delta\theta\right) = 4\cdot k_y\Delta y+2\cdot l\cdot k_y\sin\Delta\theta = F_y \quad (10)$$

where Δy and $\Delta\theta$ are the y-direction and the angular displacements, respectively and k_y is the stiffness in the y-direction. Since the displacements do not affect sliding and lifting, the equation for sliding to the right is identical to (5) and the equation for lifting is identical to (8).

For peeling of the seta, the moment is taken at the edge of the most distal spatula (see Fig. 1c for setal stalk and Fig. 1d for the spatular close-up):

$$M > \left[\Delta x+(s+l+a)\cdot\cos\Delta\theta\right]\cdot F_y - \left[h_0+(s+l+a)\cdot\sin\Delta\theta\right]\cdot F_x - \sum_{i=1}^{4} F_{iy}\frac{(l+a)\cdot(i-1)}{3} = 0 \quad (11)$$

where

$$\sum_{i=1}^{4} F_{iy}\frac{(l+a)\cdot(i-1)}{3} = \sum_{n=1}^{4} k_y\cdot\left(\Delta y+\left(\frac{n-1}{3}\right)\cdot l\cdot\sin\Delta\theta\right)\cdot\frac{(l+a)\cdot(n-1)}{3} = 2\cdot(l+a)\cdot k_y\left[\Delta y+\frac{7}{9}\cdot l\cdot\sin\Delta\theta\right] \quad (12)$$

and a is the spatular length. For a freely pivoting spatula, we choose $a = 0$.

With n = 4, the equation for setal peeling due to peeling at the fixed spatula is

$$\left[\Delta x+(s+l+a)\cdot\cos\Delta\theta\right]\cdot T\cdot\sin\phi > \left[h_0+(s+l+a)\cdot\sin\Delta\theta\right]\cdot T\cdot\cos\phi+2\cdot(l+a)\cdot k_y\cdot\left(\Delta y+\frac{7}{9}\cdot l\cdot\sin\Delta\theta\right). \quad (13)$$

After solving for Δy in (10), this Δy is substituted into (13). Simplifying (13), the equation for peeling at the fixed spatula is

$$\left[\Delta x-\frac{l+a}{2}+(s+l+a)\cdot\cos\Delta\theta\right]\cdot T\sin\phi > \left[h_0+(s+l+a)\cdot\sin\Delta\theta\right]\cdot T\cos\phi+(l+a)\cdot\left(\frac{5}{9}\cdot k_y\cdot l\cdot\sin\Delta\theta\right) \quad (14)$$

Solving for T from (14), the equation for setal peeling at the fixed spatula is

$$T > \frac{(a+l)\cdot\left(\frac{5}{9}\cdot k_y\cdot l\cdot\sin\Delta\theta\right)}{\Psi}. \quad (15)$$

where $\Psi = \left[\Delta x-\frac{l+a}{2}+(s+l+a)\cdot\cos\Delta\theta\right]\cdot\sin\phi - \left[h_0+(s+l+a)\cdot\sin\Delta\theta\right]\cdot\cos\phi$

C. *Displacement limit of compliant spatular hairs*

In the previous section, we determined the force required to peel a setal stalk. We now determine maximum allowable displacement before the peeling resistance of the seta is exceeded. For sliding, we assume a two degree of freedom model with a single bend for the spatular hair (Fig. 2). The spatular hair is modeled as a fourbar with two torsional springs at the base of the two segments [4]. The flexural pivot approach is a good approximation for smaller displacements [4].

As shown in Fig. 1c, the most proximal spatular hair is the first one to slide or peel, and its extension limit will determine the maximum setal displacement.

Assuming equal load sharing on a smooth surface, the moment balance equation to solve for the pseudo-rigid body angle Θ_1 for the top most segment of the compliant spatula is:

$$4\cdot K_1\cdot(\Theta_{1o}-\Theta_1)-TL_1\cdot\sin(\Theta_{1o}-\Theta_1-\phi) = 0 \quad (16)$$

where K_1 is the torsional spring constant and L_1 is the length for the top most segment.

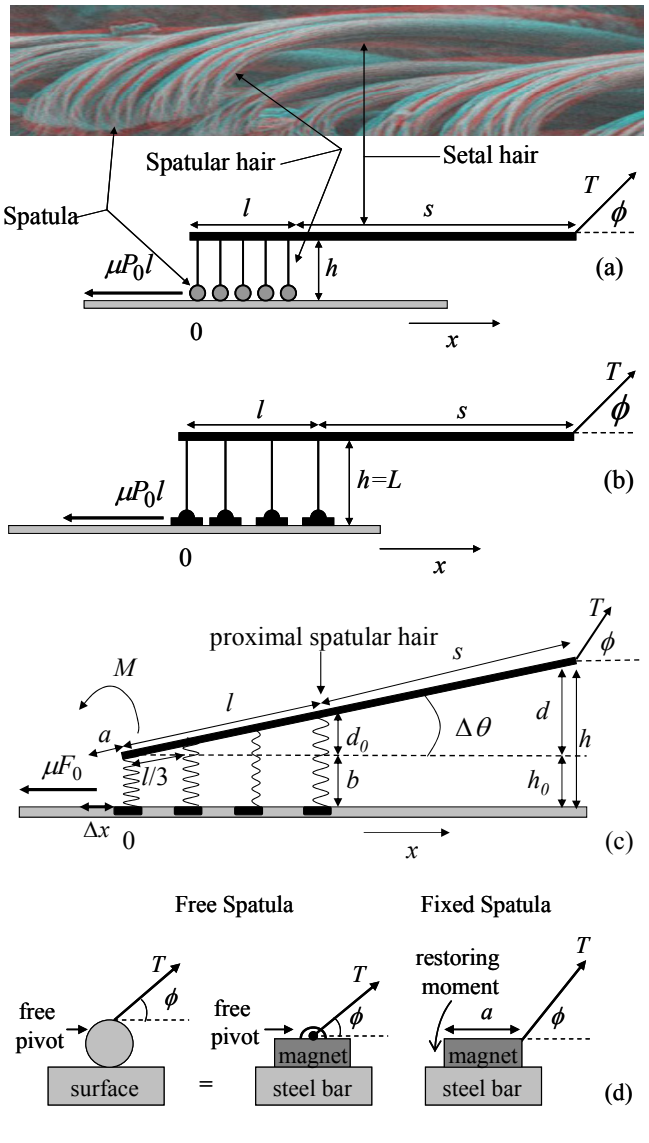

Fig. 1. Setal stalk with (a) spatular array at one end (hundreds of hairs) [from http://www.lclark.edu/~autumn/dept/Images.html], (b) with four rigid spatular hairs and (c) with four compliant spatular hairs. (d) Close-up of the free and fixed spatulae.

The moment balance equation to solve for the pseudo-rigid body angle Θ_2 for the bottom most segment of the compliant spatula is:

$$4 \cdot K_2 \cdot \left[\left(\Theta_{2o} - \Theta_2\right) - \left(\Theta_{1o} - \Theta_1\right)\right] - TL_2 \cdot \sin\left(\Theta_{2o} - \Theta_2 - \phi\right) = 0 \quad (17)$$

where K_2 is the torsional spring constant and L_2 is length for the bottom most segment. If the spatular hairs slide to the right, T satisfies (5). If setal peeling with single bent spatula hairs occurs, T satisfies (15).

The torsional spring constant is:

$$K_j = \frac{Ewt^3}{4 \cdot L_j} \quad (18)$$

where E is the elastic modulus, w is the width of the spatular leg and t is the spatular leg thickness [4].

The equations for normal position and front spatular hair displacement are given by (19) and (20) respectively:

$$b = L_1 \cdot \sin\Theta_1 + L_2 \cdot \sin\Theta_2 , \quad (19)$$

$$d_0 = L_1 \cdot \left[\sin\Theta_1 - \sin\Theta_{1o}\right] + L_2 \cdot \left[\sin\Theta_2 - \sin\Theta_{2o}\right] . \quad (20)$$

Since a long moment arm is applied as shown in Fig. 1c, the displacement by using similar triangles is

$$d = \frac{l+s}{l} \cdot d_0 = \left(l+s\right) \cdot \sin\Delta\theta . \quad (21)$$

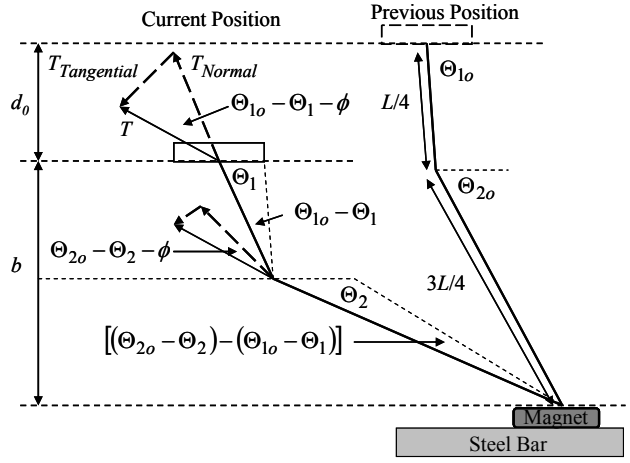

Fig. 2. Displacement diagram using the flexural pivot model for the proximal spatular hair.

Since the flexural pivot approach is a better approximation for smaller displacements, we need to account for larger displacements associated with the setal peeling of double bent spatular hairs. To account for the larger displacement, we assumed a linear spring model based on Hooke's law. To obtain the displacement, we solve for $\Delta\theta$ in (10) and substitute into (21). This displacement is complementary to the compliant setal peel force from (15).

III. Experimental Results and Comparison to Model

A. Overview of the Macromodel

Our gecko fiber macromodel comprises an array of four double bent spatular hairs. The bends occur at 1/4 and 2/3 the length of the spatular hair. The bend locations for the cases of freely pivoting and fixed spatulae are shown in Fig. 3a and Fig. 3b, respectively. The purpose of this spatular hair geometry is to have additional compliance in the vertical direction (or 90° compliance) since the straight cantilever has a very high stiffness in the normal (90°) direction.

Since the bent arrays have more compliance compared to

the straight cantilever array, bent cantilever spatular hairs extend before they pull off. The double bent shape provides an additional degree of freedom to further increase the compliance in the normal direction. To improve detachment of spatular hairs at angles greater than 90°, a long moment arm has been added to the body of the model. To understand the effects of the peeling moment at the spatula, spatular hairs containing freely pivoting and fixed spatulae were made.

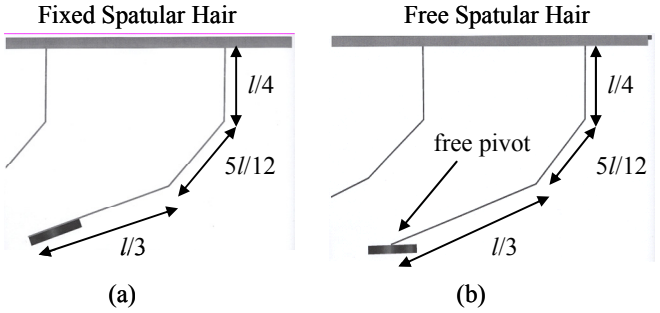

Fig. 3. Drawing of the double bent spatular hair model with (a) fixed spatula and (b) free spatula.

We also tested straight, bent and curved spatular hairs as shown in Fig. 4a-c. The actual experimental apparatus for the double bent spatular hair geometry is shown in Fig. 5a, and a close-up of the spatula is shown in Fig. 5b. The estimated stiffnesses of each spatular hair are listed in Table I.

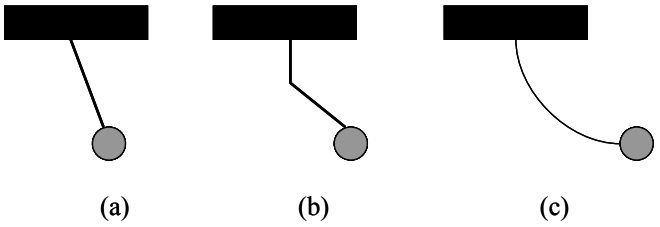

Fig. 4. Cantilever geometry for a single (a) straight, (b) bent and (c) curved spatular hair.

For the fabrication of the setal hair body, a 30 cm long foam core board (0.3 cm thickness) was bonded to a 30 cm long acrylic sheet (0.1 cm thickness) to provide a sturdy yet lightweight structure. The spatular hair legs are four 22 cm x 7 cm x 0.8 cm polycarbonate sheets which were bonded to the setal hair body.

Each of the four spatulae contained four plastic bumpers, a magnet (pull-off strength of 1.5 N per magnet) and a 4 cm long cord. One end of the cord was inserted and glued to the plastic bumpers. Then, the other end of each cord was glued and taped to the end of the legs. To obtain the fixed spatulae, the bumpers were glued to the plastic leg. The base of the setal stalk, labeled *s* in Fig. 5(a), is a 32 cm acrylic sheet glued to the body.

B. Force Limits and Comparison to Model

To measure the force, a mechanical postal scale with a relative error of 5% was used. Next, a string was tied to the scale. The magnets adhere to a 100 cm long steel bar. To control the angle, the apparatus used an elevating pulley. See Fig. 6 for a drawing of the apparatus.

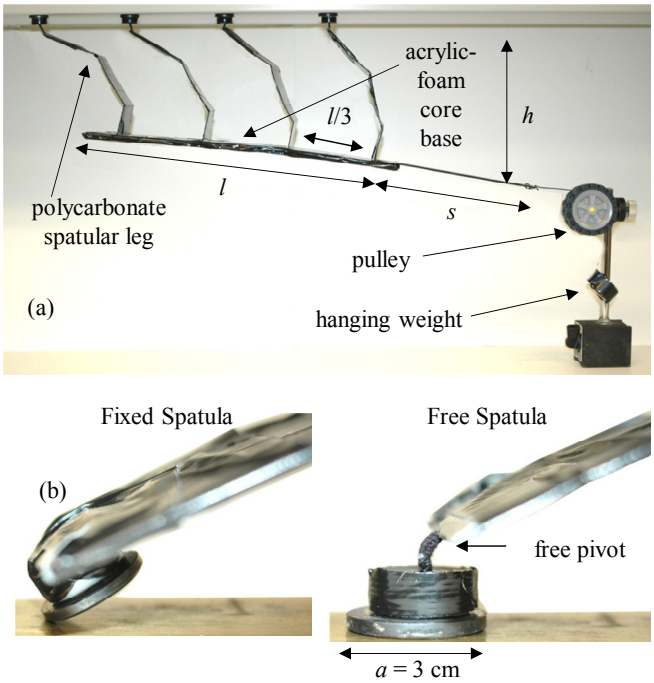

Fig. 5. (a) Actual photograph of the gecko hair macromodel with freely pivoting spatulae. (b) Actual close-up of the fixed and free spatulae.

TABLE I
STIFFNESSES OF A SINGLE FIBER ESTIMATED FROM WHOLE ARRAY

Spatular Geometry	k_x (N/cm)	k_y (N/cm)	Critical Angle (degrees)
Straight	> 13.40	> 3.00	35
Curved	9.90	2.25	35
Bent	6.60	1.50	35
Double Bent(Free)	3.30	0.75	35
Double Bent(fixed)	3.30	0.75	35

The force space plot for the double bent spatular hair model is shown in Fig. 7. Using (5), (7), (8), and (15), the intersections of each line indicate the cut-off angles for sliding, rigid peeling, lifting, compliant peeling at the free pivoting spatula and compliant peeling at the fixed spatula. These cutoff angles are listed in Table II.

From (7), (8), and (15), the double bent spatular hair model has a greater tendency to peel due to the long moment arm of the apparatus since the force required for lifting is significantly larger than the force required for peeling (either

with free or fixed spatulae). From Fig. 7, the pattern of the experimental points is more consistent with a peeling behavior than a lifting behavior. For angles between 35° and 90°, the spatular hairs peel, with the force necessary for peeling reducing at higher angles. Between 90° and 180°, the spatular hairs also peel, except the force required for peeling increases at larger angles.

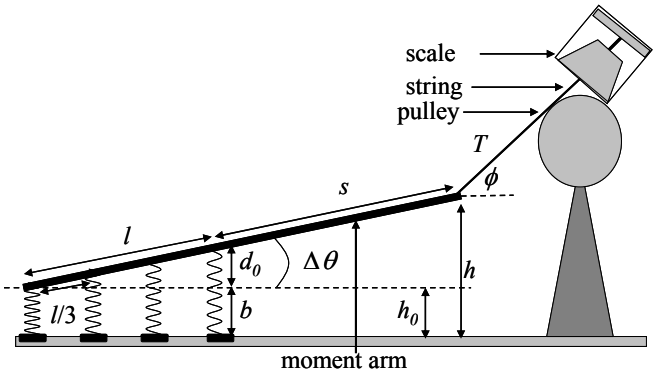

Fig. 6. Apparatus for force measurement. Note: The apparatus for displacement is almost identical except no scale is involved.

For the experimental points which correspond to peeling, we cannot conclude whether the double bent spatular hair model undergoes a rigid peel [from (7)] or a compliant peel [from (15)]. This is the case because the experimental data for the double bent spatular hair array are identical with the straight and single bent spatular hair arrays. This implies that the compliance is not high enough to significantly change the geometry.

TABLE II
CUT-OFF ANGLES FOR PULL-OFF AND SLIDING

Condition	Angle
Rigid Peel (h = 16 cm)	$35° < \phi < 180°$
Peel at the Fixed Spatula	$41° < \phi < 180°$
Peel at the Free Spatula	$38° < \phi < 180°$
Slide to Right	$0° < \phi < 35°$

Comparing (15) when $a = 0$ and $a = 3$ cm, the force for setal peeling for fixed spatulae is almost identical to the force for setal peeling for the freely pivoting spatulae. The experimental force measurements for the freely pivoting spatular hair model are slightly larger than the fixed spatular hair model because the freely pivoting spatulae aligns better with the surface.

At angles below 35°, both the mathematical model and the experimental data show sliding to the right, with the tangential force necessary for slipping reducing at higher angles. Since the coefficient of friction is measured as $\mu = 0.6$, the slide force at 0° is 3.5 N which follows the Coulomb friction model.

The predicted cutoff angle for peeling and sliding of double bent spatulae is at 35°, as listed on Table II. The experimental critical angle for this model is also 35°. This angle is the same for the straight and single bent spatulae model. From the experimental data in [3], the critical angle is between 25° and 37°. The critical angle from our experimental data is consistent with the mathematical model as well as the experimental data from [3].

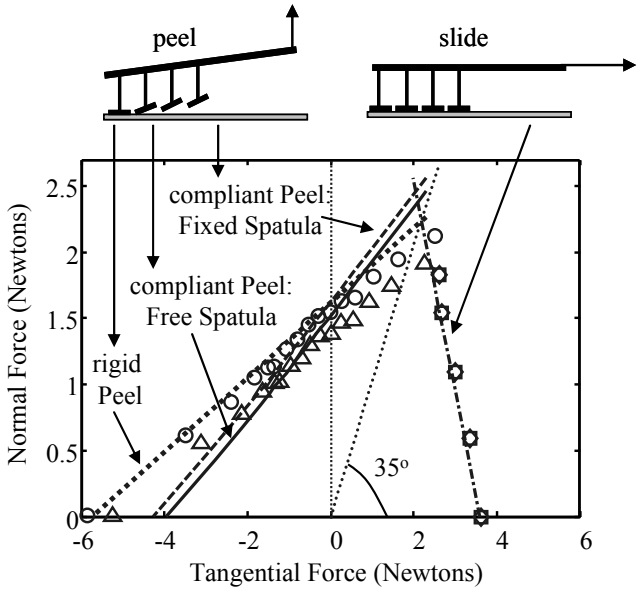

Fig. 7. Force space plot of tangential and normal forces. Experimental data: (Circle): peeling with free spatulae (Diamond): sliding of free spatulae, (Triangle): peeling of fixed spatulae, (Square): sliding of fixed spatulae.
Models: (---) compliant peel with fixed spatulae, (-) compliant peel with free spatulae, (...) rigid peel.

C. Displacement Limits and Comparison to Model

The experimental apparatus for measuring displacement limits is almost identical to the force setup. A tape marker was placed on the string to be the reference point for the measurement. A 60 cm ruler was placed on top of the string to record the initial position. The final position was recorded once the model started to slide or peel. To obtain the displacement, the difference between the final and initial measurements was taken.

For angles less than 35°, both the single bent and double bent spatular hairs slide, with the displacement increasing at higher angles. For angles between 35° and 180°, both the single and double bent spatular hairs peel, with the displacement reducing at higher angles. As shown in Fig. 8, the experimental data for sliding and single bent setal peeling is consistent with (16), (17), (20), and (21).

Between 80° and 180°, the single bent spatular hairs peel, but the displacements at those angles are higher compared to the experimental values. This result is consistent because the model spatular hair extends due to its compliance. The torsional spring equations assume that a spatular hair completely straightens to its full length under maximum displacement. Between 50° and 180°, the total displacement of the double bent spatular hairs is larger than the total displacement of the single bent spatula hair. This is consistent with linear spring model based on Hooke's law from (10), (15) and (21).

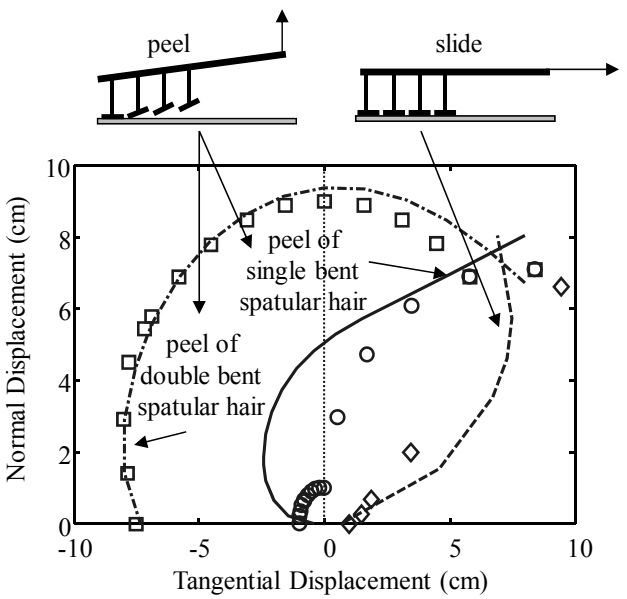

Fig. 8. Tangential and normal displacement limits. Experimental data: (Circle) single bent hair peeling, (Square) double bent hair peeling, (Diamond) single and double bent hair sliding. Models: (-) peeling of single bent spatular hair, (…) peeling of double bent spatular hair, (---) sliding.

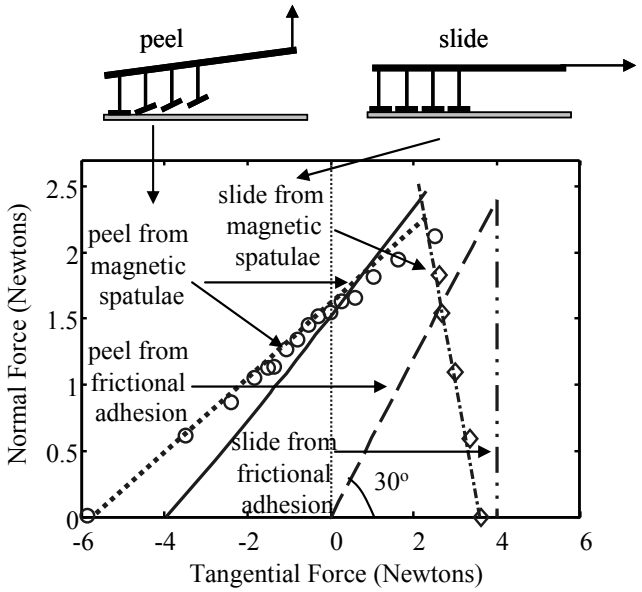

Fig. 9. Comparison of force space data and models with frictional adhesion. Experimental data: (Circle) peeling for the magnetic spatulae, (Diamond): sliding for the magnetic spatulae. Models: (---) peeling with frictional adhesion [7], (-) peeling for the magnetic spatulae. (-..) sliding with frictional adhesion.

Furthermore, the displacement of the most proximal spatular hair is almost identical for a freely pivoting spatula and a fixed spatula. This experimental data is consistent with the mathematical model which predicts that the force required for peeling with free pivoting and rigid spatulae is almost identical.

IV. Conclusion

By means of macromodels, we have approximated the mechanical behavior of gecko seta with spatular hairs. We can compare the behavior of this macromodel to the frictional adhesion behavior described in [7, 8], as shown in Fig. 9. In frictional adhesion, the normal pull-off force is reduced to zero when the tangential force is zero or negative. In our model, a non-zero peel force is required at zero normal force, but one can observe the peak peel force when a tangential force is applied. We expect that more complicated spatular geometric features will be required to demonstrate frictional adhesion.

As shown in Fig. 9, the behavior of a gecko seta with straight, single bent and double bent spatula hairs exhibit a frictional adhesion effect. Our experimental data from Fig. 8, on the other hand, demonstrate the additional compliance the double bent spatular hairs provide. From our results, the gecko seta with double bent hairs is more compliant than the other hair geometries. This extra compliance will significantly increase the work of adhesion, and make for stronger bonds, yet it does not significantly affect the peel angle. Hence, we conclude that more compliant spatular fibers are worth including in future nanofibrillar adhesives. Our results demonstrate the importance of fiber array geometry and stiffness in modeling fibrillar adhesion.

V. Acknowledgements

This material is based upon work supported by the National Science Foundation under Grant No. EEC-0304730. Any opinions, findings and conclusions or recommendations expressed in this material are those of the author(s) and do not necessarily reflect the views of the NSF.

VI. References

[1] D. Campolo, S.D. Jones and R. S. Fearing, “Fabrication of Gecko foot-hair like nano structures and adhesion to random rough surfaces”, *Proc. IEEE Nano* 2003 Aug. 12-14, San Francisco.

[2] M. Sitti and R.S. Fearing, “Synthetic gecko foot-hair micro/nano-structures for future wall climbing robots”, *Proc. IEEE Int. Conf. on Robotics and Automation*, Taiwan, May/Sept. 2003.

[3] K. Autumn, Y. Liang, T. Hsieh, W. Zesch, W.-P. Chan, T. Kenny, R. Fearing, and R.J. Full, “Adhesive force of a single gecko foot-hair”, *Nature*, vol. 405, pp. 681-685, June 8, 2000.

[4] L.L. Howell, *Compliant Mechanisms*, New York, NY: John Wiley & Sons, Inc., 2001, pp. 136-139.

[5] J. Berengueres, K. Takahashi, and S. Saito, “Magnetic hair for wall mobility”, *Proc. IEEE Int. Conf. on Intelligent Robots and Systems*, China, Oct. 2006.

[6] J. Berengueres, K. Takahashi, and S. Saito, “Structural properties of a scaled gecko foot-hair”, *Bioinsp. Biomim*. vol. 2, pp. 1-8, 2007.

[7] K. Autumn, A. Dittmore, D. Santos, M. Spenko, and M. Cutkosky, “Frictional adhesion: a new angle on gecko attachment”, *Journal of Experimental Biology* , vol. 209, pp. 3569-3579, August 11, 2006.

[8] D. Santos, S. Kim, M. Spenko, A. Parness and M. Cutkosky, “Directional adhesive structures for controlled climbing on smooth surfaces”, *Proc. IEEE Int. Conf. on Robotics and Automation*, Rome, Italy, April 2007.